A combined experimental and theoretical study of (*E*)-ethyl 3-(4-methoxyphenyl)acrylate as corrosion inhibitor of iron in 1 M HCl solutions

S. Hadisaputra,[1*] A.A. Purwoko,[1] I. Ilhamsyah,[2] S. Hamdiani,[2] D. Suhendra,[2] N. Nuryono[3] and B. Bundjali[4]

[1]*Chemistry Education Division, Faculty of Science Education, University of Mataram, Jalan Majapahit no 62 Mataram, 83125, Indonesia*
[2]*Department of Chemistry, Faculty of Mathematics and Natural Science, University of Jalan Majapahit no 62 Mataram. Mataram, 83125, Indonesia*
[3]*Department of Chemistry, Universitas GadjahMada, Sekip Utara, Yogyakarta 55281, Indonesia*
[4]*Department of Chemistry, Faculty of Mathematics and Natural Science, Institut Teknologi Bandung. Jalan Ganesha No 10 Bandung, 40132, Indonesia*
**E-mail: rizal@unram.ac.id*

Abstract

The study aimed to isolate, characterize and measure the corrosion inhibition efficiency of (*E*)-ethyl 3-(4-methoxyphenyl)acrylate (EPE) from *Kaempferia galanga* extract of iron in 1 M HCl solution. The experimental study was conducted with weight loss and electrochemical impedance measurements followed by theoretical study using density functional theory (DFT) method at the B3LYP level of theory. EPE has been successfully isolated and confirmed by spectroscopic techniques. Thermodynamic parameters: activation energy E_a, adsorption enthalpy ΔH, entropy ΔS, and Gibbs-free energy of adsorption ΔG^0_{ads} indicate physisorption mechanism. The adsorption of EPE on the iron surface follows Temkin's isothermal. It was revealed that the efficiency of corrosion inhibitor of EPE at the maximum tested concentration was 76.22%. Density functional theory (DFT) calculation of EPE was applied to compare the effect of electron donating and withdrawing groups on the efficiency of corrosion inhibitors, as an approach for designing high-efficiency new corrosion inhibitors. The corrosion inhibition performance of the EPE and its derivatives was evaluated using quantum chemical parameters such as frontier orbital energies (E_{HOMO}, E_{LUMO}), ionization potential (I), electron affinity (A), absolute electronegativity (χ), the fraction of electrons transferred (ΔN), corrosion inhibition efficiency (IE%), and binding energy (ΔE). The study shows that the corrosion inhibition efficiency of EPE increases with the addition of the NH_2 function group whereas the NO_2 group gives the opposite result.

Keywords: *corrosion inhibition, Kaempferia galanga extract, DFT.*

Received: June 23, 2018. Published: November 26, 2018 doi: 10.17675/2305-6894-2018-7-4-10

1. Introduction

Corrosion is a process of destruction of metal structures. Without prevention, corrosion leads to a massive economic loss [1]. Attempts to find eco-friendly, inexpensive and efficient corrosion inhibitors are still intensively underway. A potential candidate as a corrosion inhibitor is natural product compounds [2–6]. Natural product compounds generally utilize their heteroatom groups (O, N, and P) and their π electron to interact with metal for inhibiting corrosion processes [7]. The interaction process forms a coating on the metal surfaces, thus protecting the metal in the corrosive medium [8].

Natural product extracts as corrosion inhibitors have been widely reported and they showed high corrosion inhibitor efficiency [6–15]. However, the extracts were still a mixture of various compounds.This results in the difficulty of detecting compounds that play the most significant role as corrosion inhibitors. Furthermore, the natural product extracts corrosion inhibition efficiencies are still dependent on the plant part and location. To overcome these uncertainties and dependencies, it is necessary to isolate the pure compounds from the targeted plants. Therefore, in this work, the (*E*)-ethyl 3-(4-methoxyphenyl)acrylate (EPE) was crystallized to 99.99% purity from *Kaempferia galangal* plant extract and tested as a corrosion inhibitor.

The EPE compound itself is the lead compound of *Kaempferia galangal* plant. This plant is easy to find in almost all open area in Indonesia and most of Southeast Asia. It commonly used as herb in cooking and as a medicinal plant for a headache, stomach, asthma and anti-inflammatory. EPE is likely to have potential as an anti-corrosion agent due to the presence of benzene rings as a π electron donor and oxygen heteroatom within its framework that causes EPE to interact strongly with metal surfaces. In the present study, corrosion inhibition performances and thermodynamic adsorption of EPE were assessed using weight loss, electrochemical impedance measurements and theoretical studies. DFT study was applied to predict and to explain the structural relationship of EPE and its derivatives to their anti-corrosion properties.

2. Methods and Procedures

2.1 Materials

All chemicals are ordered from Sigma Aldrich/Indonesia and used without further purification. Fourier Transform Infrared (FTIR) spectra were obtained by a Shimadzu FTIR-8300 spectrometer. Nuclear Magnetic Resonance spectra were recorded on ^{1}H NMR 500Hz JEOL Spectroscopy. Gas Chromatography-Mass Spectroscopy GC-MS QP2010 Shimadzu was also used.

2.2 Extraction

A dry powder of *Kaempferia galangal* was extracted using *n*-hexane by soxhlet extraction technique. The soxhlet result was then evaporated to obtain the filtrate using a vacuum

rotary evaporator. The filtrate was then cooled to 2°C overnight until EPE crystals are formed. The formed crystals were then purified by recrystallization. Needle-like white crystals of EPE are formed with a melting point of 52°C. Characterization is then performed using FTIR, ^{1}H NMR and GC-MS. FTIR spectrum: C=O 1704 cm^{-1}; C–O 1367–1321 cm^{-1}; C=C aryl 1629–1573 cm^{-1}; C–H aryl 3007–3045 cm^{-1}; C–H aliphatic 2979–2842 cm^{-1}; C–O aryl 1252–1210 cm^{-1}; aromatic *para* position 829 cm^{-1}. ^{1}H NMR 1.33 ppm (t, 3H, J = 7.15); 4.25 ppm (q, 2H, J = 7.15); 6.31 ppm (d, 1H, J = 15.6); 7.65 ppm (d, 1H, J = 16.25); 6.90 ppm (d, 2H, J = 9.05); 7.47 ppm (d, 2H, J = 8.45); 3.82 ppm (s, 3H). Molecular weight = 206.24 g·mol^{-1}.

2.3 Weight Loss Measurement

The iron specimens were made with an effective area of 1 cm^2, and iron sample was suspended in 100 mL of 1 M HCl solution with or without an inhibitor. The inhibitor concentrations studied were 4.85×10^{-4} M, 9.7×10^{-4} M, 1.4×10^{-3} M and 1.9×10^{-3} M. After 1, 2, 3, 4, 12, 24 and 24 hours of immersion, the sample was washed, dried, and weighed. The inhibition efficiencies (IE%) were calculated using Eq. 1.

$$IE\% = \left(1 - \frac{w_2}{w_1}\right) \times 100\% \quad (1)$$

where w_1 and w_2 are the lost weight of the iron specimen in the absence and presence of an inhibitor, respectively.

2.4 Electrochemical Impedance Measurements

The surface preparation of the iron electrode was conducted by silica carbide paper 800 and 2000 grid, and re-washed using distilled water and ethanol before use. Furthermore, the electrodes are connected with a potentiostat PG PG 301. Hydrochloric acid solutions were prepared from concentrated acid and double distilled water. The solutions were prepared by mixing hydrochloric acid with the inhibitors, which used without any pretreatment. Addition of inhibitor solution was carried out on various concentrations of 7.27×10^{-4} M, 9.69×10^{-4} M, 1.21×10^{-3} M and 1.45×10^{-3} M at 298 K, 308 K and 318 K. The analysis begins with the EIS potential open circuit measurement at a frequency of 10 kHz – 100 mHz.

2.5 Computational details

EPE geometry was optimized using the DFT/B3LYP level of theory. The LANL2DZ basis set was used for Fe and 6-31G (d) basis set for EPE. The polarized continuum model (PCM) was used to calculate the solvent effects due to corrosion dominantly occurred in the aqueous environment. To determine the energy of the interaction, the re-optimization of the structure was not performed on the solvent because it had little effect on the energetic so that it was sufficient to use single-point calculations on gas-phase geometries

[17–20]. All theoretical calculations are performed with the Gaussian 03 package [21]. The quantum chemical parameters (E_{HOMO}), the energy of the lowest molecular orbitals (E_{LUMO}), the ionization potential (I), the electron affinity (A), the absolute electronegativity (χ) , hardness (η), softness (σ), the fraction of electron transferred (ΔN), and the theoretical corrosion inhibitor efficiency (IE_{theory}%) were calculated as previously reported equations [22–24].

3. Results and discussion

3.1 Isolation and characterization

Isolation of EPE compound (Figure 1) produced white crystal with *Kaempferia galangal* typical aroma with a yield of 85.74%. The crystals were then identified using thin layer chromatography (TLC). The retention factor value of the TLC sample is equal to the standard retention factor value of 0.694. The crystal has a melting point of 52°C. To strengthen the identification results, further analysis was performed using FTIR, ^{1}H NMR and GC-MS. FTIR spectrum shows the presence of carbonyl group (C=O) at 1704.1 cm^{-1}, aryl group (C=C) at 1629.9–1573.0 cm^{-1}, CH aliphatic 2979.18–2842.2 cm^{-1}, CO aryl 1252.8–1210.4 cm^{-1} and aromatic *para* position at 829.43 cm^{-1}. Proton NMR spectrum exhibited weak triplet signal (3H) at 1.33 ppm and quartet at 4.25 ppm (2H). The chemical shift for a *trans*-configured olefin was at 6.31 ppm (doublet 2H) associated with a chemical shift of 7.65 ppm (doublet 2H) with coupling constants of 15.6 and 16.25, respectively. Proton benzene is shown by 6.90 ppm (doublet, 2H, J = 9.05) and 7.47 ppm (doublet, 2H, J = 8.45). The singlet signal (3H) for hydrogen methoxy at 3.82 ppm. The GS-MS spectra show a retention time of 9.9 with a molecular weight of 206.24 g·mol^{-1} and mass fragmentation at 161,134, 118, 103, 69, 63 and 39 g·mol^{-1}. The characterization data confirm that the isolated compound was EPE with 99.99% purity.

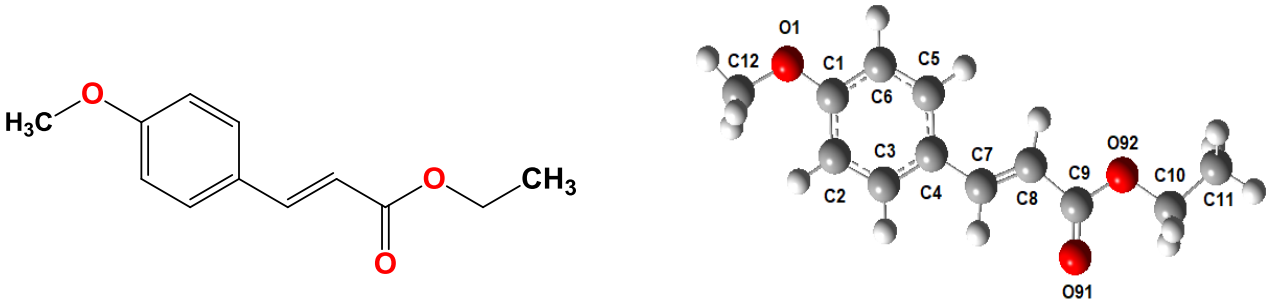

Figure 1. The 2D structure of (*E*)-ethyl 3-(4-methoxyphenyl)acrylate (EPE) and the optimized structure of EPE molecule determined using DFT method.

3.2 Weight loss studies

The corrosion inhibition efficiency of EPE was assessed by weight loss measurements at various concentrations (7.27×10^{-4} M, 9.69×10^{-4} M, 1.21×10^{-3} M and 1.45×10^{-3} M) at 308 K after 1, 2, 3, 4, 12, 24 and 24 hours of immersion. The inhibition efficiencies EPE

compounds by weight loss measurement for 308 K are depicted in Figure 2. Figure 2 indicates that EPE reduced the iron corrosion in acidic medium. The inhibitor efficiency increased with the increasing inhibitor concentration. The high corrosion inhibition efficiency of EPE indicates that it has a high bonding ability to iron surface. The EPE bonding on iron surfaces possible due to EPE has oxygen heteroatoms and aromatic benzene rings that donate π electrons to the formation of physisorption on the surface of the iron.

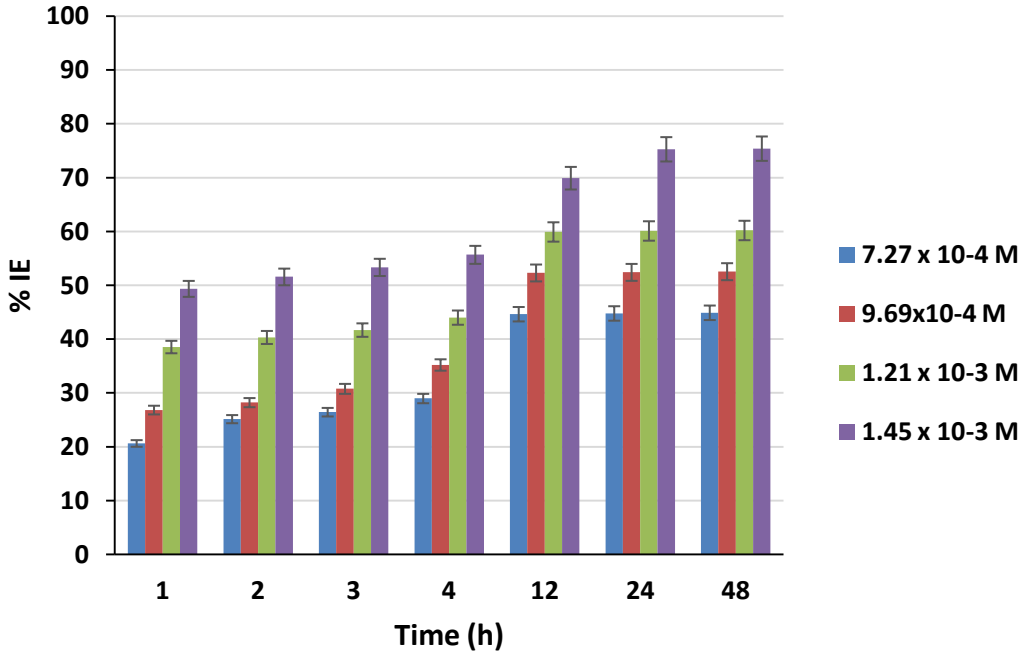

Figure 2. EPE inhibition efciency for iron as a function of time at various inhibitor concentrations (7.27×10^{-4} M, 9.69×10^{-4} M, 1.21×10^{-3} M and 1.45×10^{-3} M) and temperature 308 K.

3.3 Electrochemical impedance spectroscopy (EIS)

Figure 3 shows the Nyquist curve from the efficiency test of corrosion inhibitors of EPE compounds at various temperatures and concentrations. From the Nyquist curve in Figure 3 shows that the impedance response of iron has significantly change after the addition of various EPE concentrations. EPE has the ability to inhibit corrosion shown by enlarging the semicircular curve on the Nyquist curve along with the addition of inhibitor concentration. At the lowest inhibitor concentration, EPE has also actively inhibited corrosion in 1 M HCl. Table 1 shows the charge transfer resistance, double layer capacitance, and the efficiency of corrosion inhibitors from EPE molecule based on the Nyquist curve. It shows that the double layer capacitance C_{dl} decreased as the concentration of EPE increased. Thus, the inhibition efficiency increased. The C_{dl} decrease, as a result from an increase in the thickness of the electric double layer and a decrease in

local dielectric constant, indicated that EPE molecules function by adsorption at the solution/interface [25].

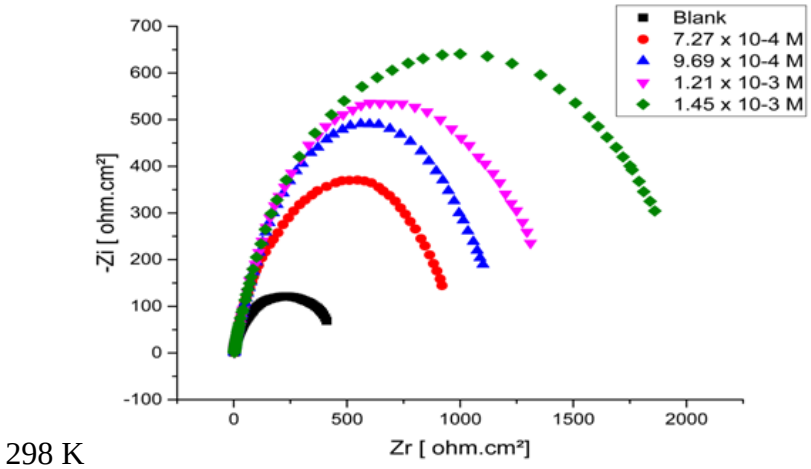

298 K

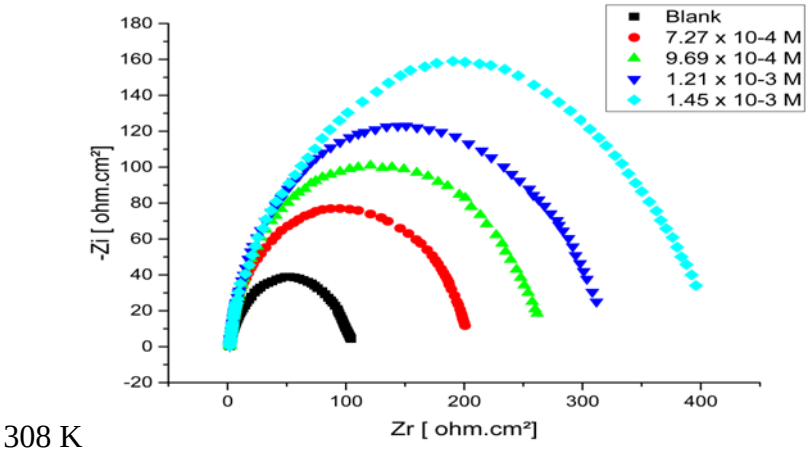

308 K

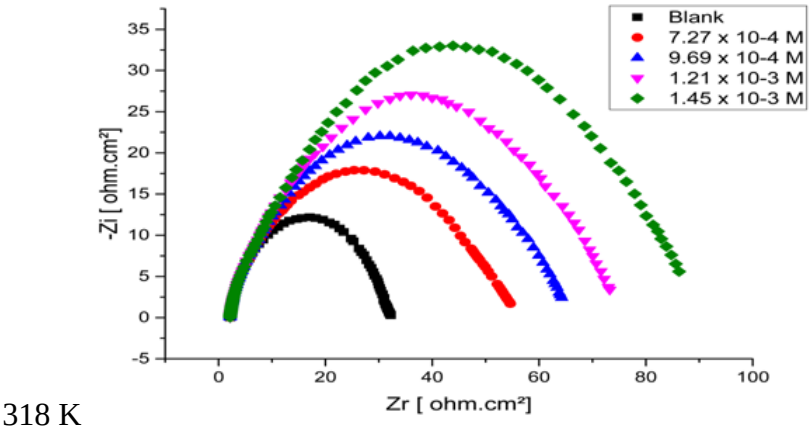

318 K

Figure 3. Iron Nyquist diagrams at various concentration of EPE (7.27×10^{-4} M, 9.69×10^{-4} M, 1.21×10^{-3} M and 1.45×10^{-3} M) and temperature (298 K, 308 K, 318 K).

Table 1. Impedance parameters for iron in 1 M HCl solution with and without different concentrations of the investigated inhibitors at 298 K, 308 K and 318 K.

T (K)	C (M)	R_s (Ω cm^2)	R_{ct} (Ω cm^2)	C_{dl} (μF cm^{-2})	f(Hz)	θ	%IE
298	blank	2.812	448.8	245.68	1.44	–	–
	7.27×10^{-4}	2.866	933.2	53.88	3.17	0.5191	51.9074
	9.69×10^{-4}	2.662	1246.7	46.54	2.74	0.6400	64.0010
	1.21×10^{-3}	2.512	1416.7	45.31	2.48	0.6832	68.3207
	1.45×10^{-3}	2.468	1887.9	39.43	2.14	0.7623	76.2276
308	blank	1.812	103.0	153.97	1.00	–	–
	7.27×10^{-4}	2.126	202.9	71.17	1.10	0.4924	49.2361
	9.69×10^{-4}	1.967	258.5	56.94	1.08	0.6014	60.1547
	1.21×10^{-3}	1.954	312.1	50.1	1.02	0.6700	66.9978
	1.45×10^{-3}	1.847	396.2	40.05	1.01	0.7600	74.003
318	blank	2.168	30.0	274.76	1.93	–	–
	7.27×10^{-4}	2.054	54.5	74.96	3.89	0.4516	45.1554
	9.69×10^{-4}	1.973	63.9	70.65	3.53	0.5307	53.0736
	1.21×10^{-3}	1.942	71.4	68.43	3.26	0.5804	58.0392
	1.45×10^{-3}	1.870	85.7	62.56	2.97	0.6504	65.0408

3.4 Thermodynamic of adsorption

The interaction mechanism between EPE and iron was then studied using thermodynamic studies. Thermodynamic factors such as activation energy, enthalpy, entropy changes, and adsorption-free energy can be used to determine the inhibition process. Activation energy (E_a) is the minimum energy required for the ongoing chemical reaction. E_a value indicates that the higher the concentration the greater the activation energy required. The greater E_a value indicates a greater energy barrier to inhibit the oxidation reaction in the corrosion process. The Arrhenius equation shows that the current density is inversely proportional to E_a exponential. This means that the bigger the E_a value the smaller the corrosion rate. The E_a value < 80 kJ indicates the occurrence of physical adsorption while the value of E_a > 80 kJ indicates the occurrence of chemical adsorption [26]. It was found that the E_a value was 23.58 kJ·mol^{-1} at 1.45×10^{-3} M means that the adsorption of EPE on ion surface featuring physisorption mechanism.

The higher the enthalpy value the more difficult the corrosion occurs because it requires greater energy. The value of enthalpy increases as the inhibitor concentration increases. The enthalpy values for the concentrations of 7.27×10^{-4}, 9.69×10^{-4}, 1.21×10^{-3} and 1.45×10^{-3} M are 44.60, 46.20, 48.04, 55.26 kJ·mol^{-1}, respectively. The value of the

enthalpy is positive so that corrosion procession is endothermic due to the presence of inhibitor. The value of entropy increases as the inhibitor concentration increases by 23.16, 24.12, 24.89 and 31.40 $J \cdot mol^{-1} \cdot K^{-1}$, respectively. The value of the adsorption entropy is also positive, meaning that the adsorption occurs spontaneously.

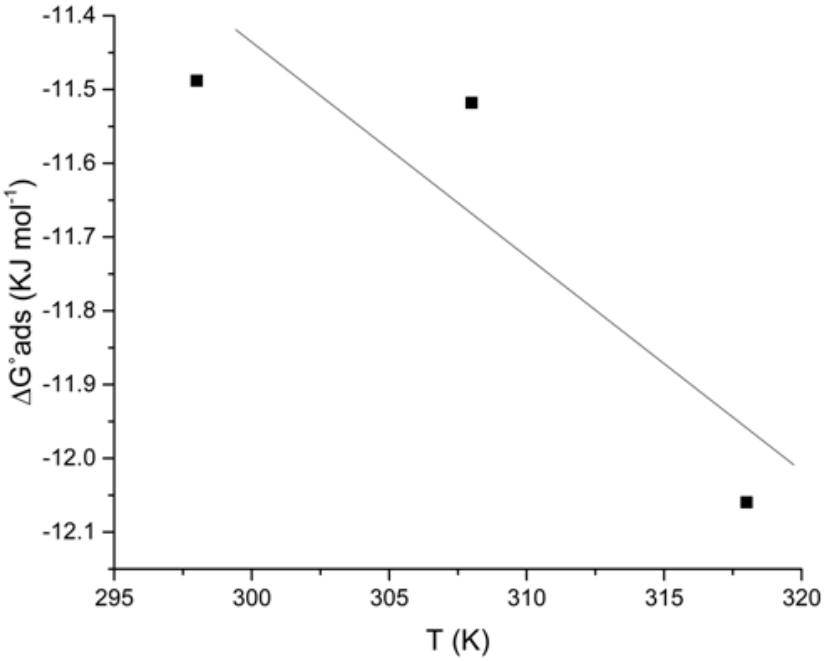

Figure 4. The relationship between ΔG^0_{ads} and *T* for EPE in 1 M HCl solution.

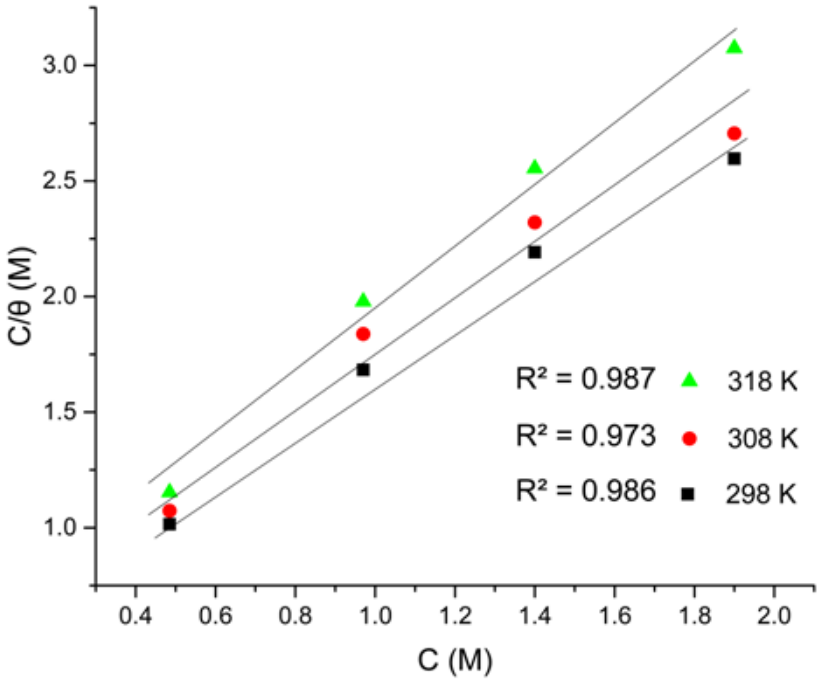

Figure 5. Temkin adsorption isotherm of EPE on iron surfaces in 1 M HCl at different temperatures.

Information on the interaction mechanism between an inhibitor and metal surfaces is obtained from isothermal adsorption. The surface coverage value (θ) of EPE at various concentrations has been tested according to the best isothermal conditions including Langmuir, Temkin, Freundlich. Plot θ *vs* ln*C* at different temperatures gives a straight line as shown in Figure 4. Thus, the best fit is obtained from Temkin adsorption. Isothermal Temkin identifies that EPE adsorption on iron surfaces is multilayer and more likely to be physisorption. The physisorption adsorption process is also indicated by the value of $-\Delta G^0_{ads} < -20$ kJ·mol^{-1} and the negative value indicates the reaction is spontaneous.

3.5 Density functional theory calculation

In this work, theoretical calculations are used to predict EPE derivatives with higher efficiency corrosion inhibition. Here, we tested three potential EPE derivatives as corrosion inhibitors (*E*)-ethyl 3-(2-amino-4-methoxyphenyl)acrylate (EPE–NH_2), (*E*)-3-(4-methoxyphenyl)acrylic acid (EPECOOH), and (*E*)-ethyl 3(4-methoxy-2-nitrophenyl)acrylate (EPE–NO_2).The structures and optimized geometries of the studied molecules are depicted in Figure 6.

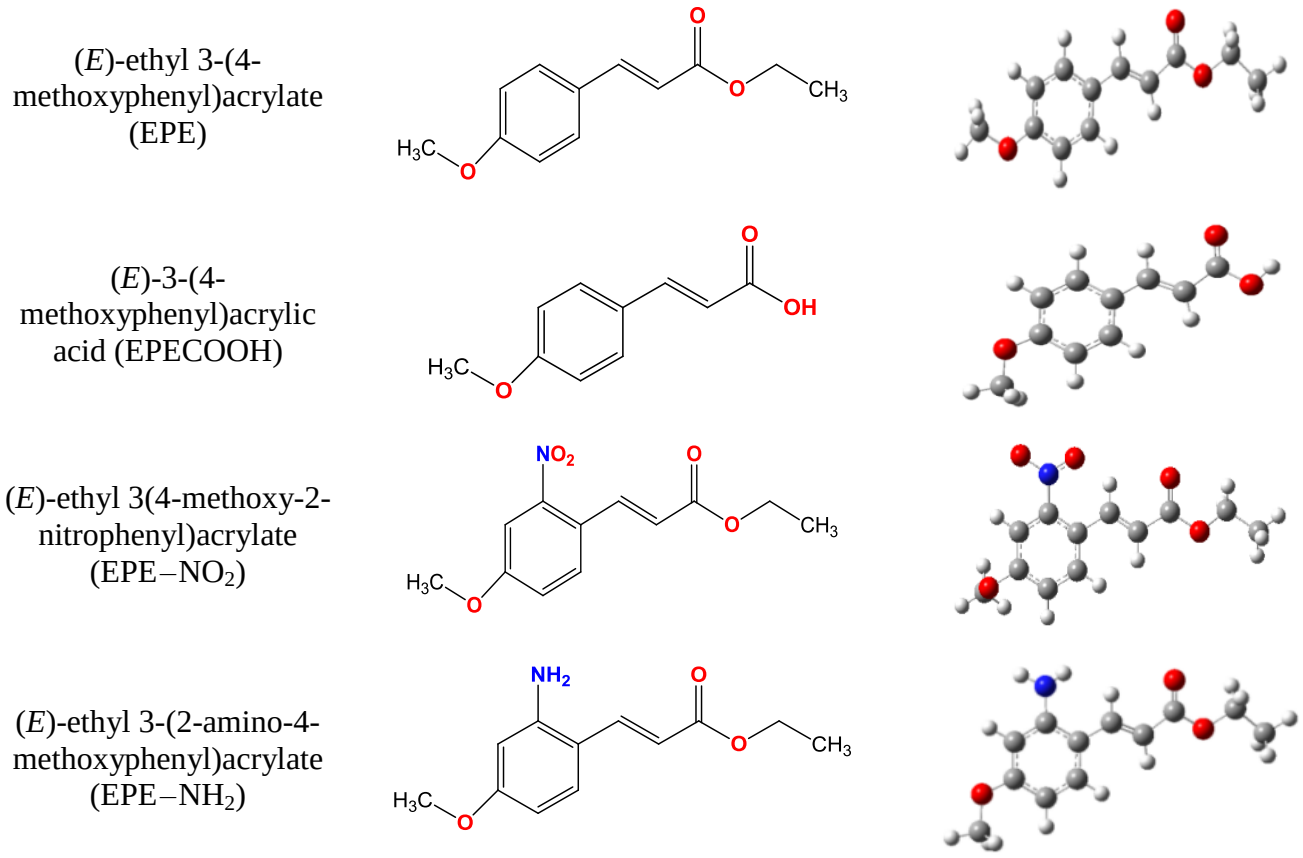

Figure 6. 2D and optimized structures of EPE and its derivatives.

As a consequence of applying density functional theory method, it is necessary to validate the level of theory by comparing theoretical results with the experimental parameters. The optimized structure of EPE compounds was compared with its X-ray crystal structure [27]. Comparison of experimental and theoretical geometrical parameters of EPE compounds was presented in Table 2. The geometrical structure of theoretical calculation agrees with the experimental data. The theoretical bond length of C1–O1 was 1.368 Å while the experiment was 1.361 Å. The similar trend was shown by the theoretical and experimental bond angle whereas O1–C1–C6 angles were 115.5° and 115.7°, respectively. It showed that DFT/B3LYP method with 6-31G (d) basis set can be applied in this research due to it is time efficient and accurate. Table 3 shows the parameters of quantum descriptors, corrosion inhibitor efficiencies and binding energies of the EPE and its derivatives obtained from B3LYP/6-31G (d) level of theory.

Table 2. Comparison of geometrical parameters of EPE between experimental and theoretical calculation.

Bond Length	**Exp* (Å)**	**DFT (Å)**	**Bond Angle**	**Exp* (Å)**	**DFT (Å)**
C1–O1	1.368	1.361	O1–C1–C2	124.2	123.5
C1–C2	1.381	1.404	O1–C1–C6	115.5	115.7
C1–C6	1.381	1.411	C2–C1–C6	120.3	119.5
O1–C12	1.420	1.419	C1–O1–C12	118.5	118.5
C2–C3	1.392	1.399	C1–C2–C3	118.7	119.3
C3–C4	1.382	1.407	C2–C3–C4	122.1	122.0
C4–C5	1.394	1.417	C3–C4–C5	117.7	117.4
C4–C7	1.471	1.461	C3–C4–C7	119.3	119.0
C5–C6	1.377	1.387	C5–C4–C7	122.9	123.4
C7–C8	1.319	1.352	C4–C5–C6	121.0	121.2
C8–C9	1.475	1.478	C1–C6–C5	120.2	120.3
C9–$O9_{(1)}$	1.201	1.220	C4–C7–C8	127.7	127.7
C9–$O9_{(2)}$	1.335	1.359	C7–C8–C9	120.6	120.1
$O9_{(2)}$–C10	1.458	1.441	C8–C9–$O9_{(1)}$	124.9	126.2
C10–C11	1.479	1.518	C8–C9–$O9_{(2)}$	111.5	110.5

The effectiveness of corrosion inhibitors depends not only on spatial molecular structures but also on the nature of molecular electronic structures. The high occupied molecular orbital (HOMO) and low unoccupied molecular orbital (LUMO) energies related to the reactivity of the EPE. The interaction between E_{HOMO} and E_{LUMO} of reacting species lead to the transition of electrons within molecules [28]. The transition of electrons, including donation and acceptance, are measured by the energy value of molecular orbitals.

The HOMO energy indicates the tendency of molecules towards the donation of electrons. It is found that EPE–NH_2 has higher HOMO energies than EPE, EPECOOH, and EPE–NO_2. Therefore, EPE–NH_2 is more intent on donating electrons than EPE, EPECOOH, and EPE–NO_2. This trend explains why EPE–NH_2 has higher corrosion inhibition efficiency.

The potential value of ionization (*I*) describes the reactivity of a molecule. A low ionization potential value indicates a molecule has a low reactivity [29]. Low reactivity signifies a stable molecule, so the lower the reactivity of a molecule the higher the inhibition efficiency. Inhibition efficiency follows the increasing sequence of ionization potential values, where EMPS–NH_2 has a lower ionization potential than EPE, EPECOOH, and EPE–NO_2. This explains why the addition of an electron donor NH_2 group increases the EPE corrosion inhibitor.

Table 3. The quantum chemical parameters, corrosion inhibitor efficiencies and bindingenergies of the EPE and its derivatives obtained from DFT/B3LYP/6-31G(d) level of theory.

Parameters	**Inhibitors**			
	EPE	**EPECOOH**	**EPE–NH_2**	**EPE–NO_2**
E_{HOMO} (eV)	–6.0635	–6.0807	–5.6867	–6.5362
E_{LUMO} (eV)	–1.8964	–1.9453	–1.8357	–2.9715
E_{gap} (eV)	–4.1672	–4.1353	–3.8510	–3.5647
I (eV)	6.0635	6.0807	5.6867	6.5362
A (eV)	1.8964	1.9453	1.8357	2.9715
χ (eV)	3.9799	4.0130	3.7612	4.7538
ΔN	0.7247	0.7223	0.8411	0.6301
IE_{theory}%	76.2276	75.4731	80.4611	69.7064
ΔE (kJ·mol^{-1})	–165.95	–170.18	–175.56	–170.46

Electronegativity indicates the level of stability of the molecule. A small electronegativity value causes the molecule to easily achieve stability [27]. Table 3 shows the order of increase of the electronegativity values as follows EPE–NO_2 > EPECOOH > EPE > EPE–NH_2. The electronegativity value of EPE–NH_2 is 3.7612 eV, this value is lower than EPE–NO_2 of 4.7538 eV. This electronegativity shows that the inhibition efficiency of EPE–NH_2 is higher than that of EPE–NO_2.

The number of electrons transferred (ΔN) is also depicted in Table 3. Based on Lukovits's study [28], if the ΔN value < 3.6, the efficiency of the inhibitor will increase its due dilution of electrons to the metal surface. The greater the value of ΔN, the greater the ability of the inhibitor to donate electrons to the metal surface. This shows that the EPE–NH_2 has the least fraction of electrons efficiency, whereas EPE–NO_2 has the least fraction, and this is associated with the least inhibitor efficiency.

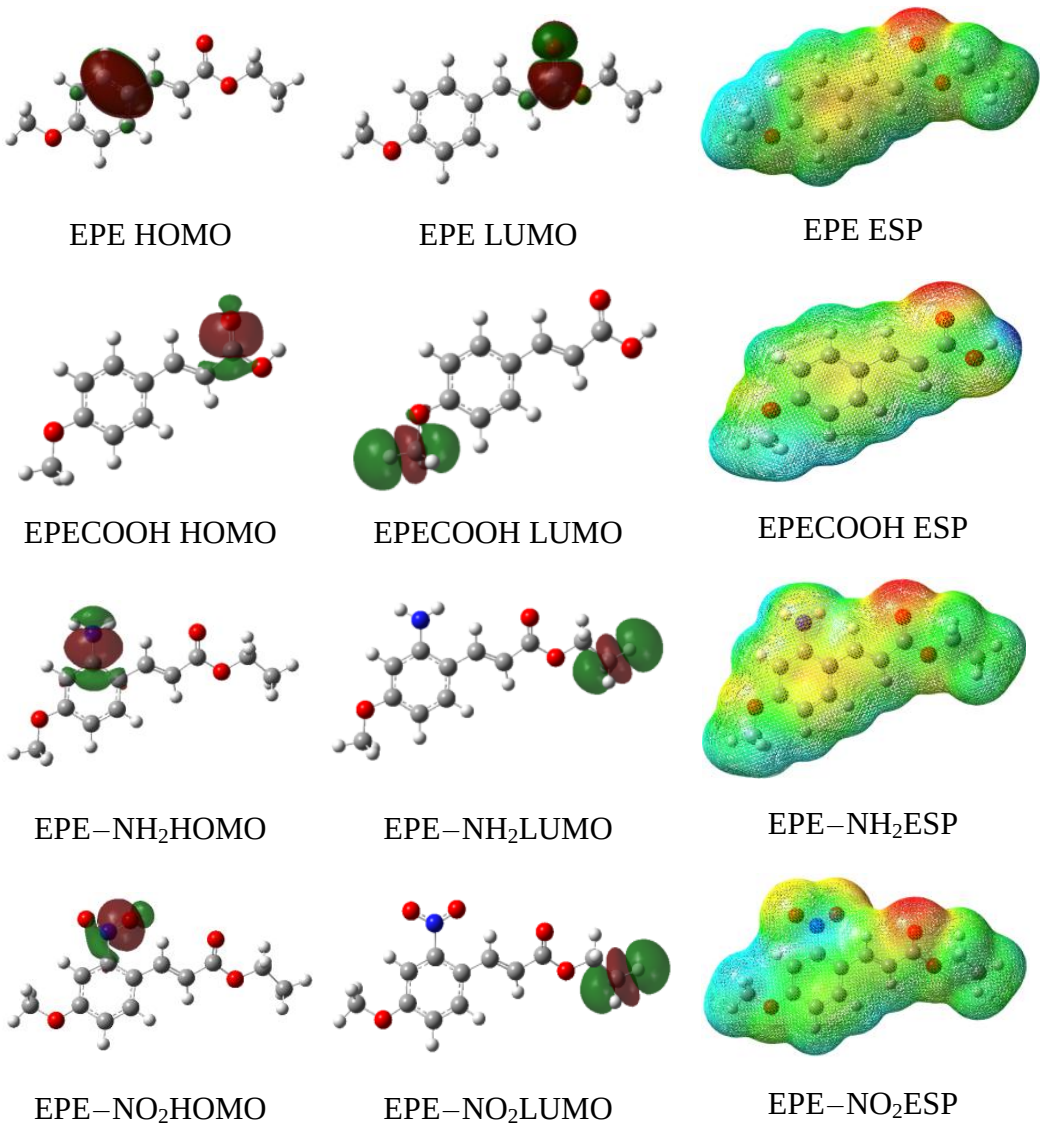

Figure 7. Optimized geometries, HOMOs, LUMOs and electrostatic potential maps of EPE and its derivatives obtained with DFT/B3LYP/6-31G(d) level of theory.

The addition of substitution groups to EPE effect the efficiency of corrosion inhibition. Increased efficiency of EPE corrosion inhibition and its derivatives are sorted as follows: EPE–NO_2 < EPECOOH < EPE < EPE–NH_2. The sequence of the efficiency of this corrosion inhibitor correlates linearly with quantum chemical parameter values. The addition of substitution groups has an effect on the efficiency of corrosion inhibition due to differences in electron and electrostatic distribution in studied molecules as shown in Figure 7. In EPE–NH_2, the nucleophile difference is centered on NH_2 (base donor power 7.27) and in EPE–NO_2 centered only on C=O. The yellow and red colors that dominate on EPE–NH_2 show more electron charge distribution whereas in EPE–NO_2 displays the dominance of green and blue. This means that EPE–NH_2 is nucleophilic and EPE–NO_2 is electrophilic. As a result, EPE–NH_2 bonds better on the surface of iron than EPE–NO_2 so that it is able to inhibit corrosion process better.

The interaction energy between EPE and iron molecules was calculated. The interaction energy values show the complex stability formed between EPE and iron. The more negative the interaction energy is, the more stable the complex. The order of complex stability between EPE and its derivatives with iron is EPE–NH_2 > EPE–NO_2 > EPECOOH > EPE (Table 3). The value of the interaction energy correlates well with the efficiency value of theoretical inhibition ($IE_{Theor.}$%). The addition of electron donor NH_2 groups increases the complex stability and the efficiency of corrosion inhibition is also increased.

4. Conclusion

The experimental and theoretical studies of (*E*)-ethyl 3-(4-methoxyphenyl)acrylate (EPE) as corrosion inhibitors have been performed. Calculation of corrosion inhibition efficiency is done by weight loss method and electrochemical impedance measurements. The optimum inhibition efficiency was 76.22% at 1.45×10^{-3} M. Isothermal adsorption follows the Temkin adsorption multilayer featuring physisorption mechanism. Theoretical study was conducted to find candidate potential EPE-based inhibitors with higher IE% value. The efficiency of corrosion inhibition of EPE and its derivatives correlates well with quantum descriptor parameters such as the frontier molecular orbital (E_{HOMO} and E_{LUMO}), energy gaps (E_{gap}), ionization potential (I), electron affinity (A), electronegativity (χ), and electron transfer (ΔN). The addition of the NH_2 group increased the efficiency of corrosion inhibition by up to 80.46%.

Acknowledgments

This research was financially supported by PDUPT RISTEKDIKTI 2018 Indonesia grant number: 732.UN18.L1/PP/2018, and their support is gratefully acknowledged.

References

1. G. Trabanelli, *Corrosion*, 1991, **47**, 410–419. doi: 10.5006/1.3585271
2. V. Vorobyova, O. Chygyrynets', M. Skiba, T. Zhuk, I. Kurmakova and O. Bondar, *Int. J. Corros. Scale Inhib.*, 2018, **7**, no. 2, 185–202. doi: 10.17675/2305-6894-2018-7-2-6
3. C.O. Akalezi, C.E. Ogukwe, E.A. Ejele and E.E. Oguzie, *Int. J. Corros. Scale Inhib.*, 2016, **5**, no. 3, 232–247. doi: 10.17675/2305-2016-5-3-4
4. A.S. Fouda, H.M. El-Abbasy and A.A. El-Sherbini, *Int. J. Corros. Scale Inhib.*, 2018, **7**, no. 2, 213–235. doi: 10.17675/2305-6894-2018-7-2-8
5. A. Ehsani, M.G. Mahjani, M. Hosseini, R. Safari, R. Moshrefi and H.M. Shiri, *J. Colloid Interface Sci.*, 2017, **490**, 444–451. doi: 10.1016/j.jcis.2016.11.048
6. P.E. Alvarez, M.V. Fiori-Bimbi, A. Neske, S.A. Brandán and C.A. Gervasi, *J. Ind. Eng. Chem.*, 2018, **58**, 92–99. doi: 10.1016/j.jiec.2017.09.012
7. C. Verma, M.A. Quraishi, E.E. Ebenso and I. Bahadur, *J. Bio Tribo Corros.*, 2018, **4**, no. 3, 33. doi: 10.1007/s40735-018-0150-3

8. Y. Qiang, S. Zhang, B. Tan and S. Chen, *Corros. Sci.*, 2018, **133**, 6–16. doi: 10.1016/j.corsci.2018.01.008
9. F.E.T. Heakal, M.A. Deyab, M.M. Osman and A.E. Elkholy, *Desalination*, 2018, **425**, 111–122. doi: 10.1016/j.desal.2017.10.019
10. M. Srivastava, P. Tiwari, S. Srivastava, A. Kumar, G. Ji and R. Prakash, *J. Mol. Liq.*, 2018, **254**, 357–368. doi: 10.1016/j.molliq.2018.01.137
11. E. Ituen, O. Akaranta, A. James and S. Sun., *Sustainable Mater. Technol.*, 2017, **11**, 12–18. doi: 10.1016/j.susmat.2016.12.001
12. G. Ji, S. Anjum, S. Sundaram and R. Prakash., *Corros. Sci.*, 2015, **90**, 107–117. doi: 10.1016/j.corsci.2014.10.002
13. M. Faustin, A. Maciuk, P. Salvin, C. Roos and M. Lebrini, *Corros. Sci.*, 2015, **92**, 287–300. doi: 10.1016/j.corsci.2014.12.005
14. P. Mourya, S. Banerjee and M.M. Singh, *Corros. Sci.*, 2014, **85**, 352–363. doi: 10.1016/j.corsci.2014.04.036
15. A. Singh, I. Ahamad and M.A. Quraishi, *Arab. J. Chem.*, 2016, **9**, S1584–S1589. doi: 10.1016/j.arabjc.2012.04.029
16. N. El Hamdani, R. Fdil, M. Tourabi, C. Jama and F. Bentiss, *App. Surf. Sci.*, 2015, **357**, 1294–1305. doi: 10.1016/j.apsusc.2015.09.159
17. S. Hadisaputra, L.R. Canaval, H.D. Pranowo and R. Armunanto, *Monatsh. Chem.*, 2014, **145**, no. 5, 737–745. doi: 10.1007/s00706-013-1129-x
18. A.A. Purwoko and S. Hadisaputra, *Orient. J. Chem.*, 2017, **33**, no. 2, 717–724. doi: 10.13005/ojc/330218
19. S. Hadisaputra, L.R. Canaval, H.D. Pranowo and R. Armunanto, *Indones. J. Chem.*, 2014, **14**, no. 2, 199–208. doi: 10.22146/ijc.844
20. S. Hadisaputra, H.D. Pranowo and R. Armunanto, *Indones. J. Chem.*, 2012, **12**, no. 3, 207–216. doi: 10.22146/ijc.715
21. M.J. Frisch, G.W. Trucks, H.B. Schlegel, G.E. Scuseria, M.A. Robb, J.R. Cheeseman, J.A. Montgomery, T.J. Vreven, K.N. Kudin, J.C. Burant, J.M. Millam, S.S. Iyengar, J. Tomasi, V. Barone, B. Mennucci, M. Cossi, G. Scalmani, N. Rega, G.A. Petersson, H. Nakatsuji, M. Hada, M. Ehara, K. Toyota, R. Fukuda, J. Hasegawa, M. Ishida, T. Nakajima, Y. Honda, O. Kitao, H. Nakai, M. Klene, X. Li, J.E. Knox, H.P. Hratchian, J.B. Cross, C. Adamo, J. Jaramillo, R. Gomperts, R.E. Stratmann, O. Yazyev, A.J. Austin, R. Cammi, C. Pomelli, J.W. Ochterski, P.Y. Ayala, K. Morokuma, G.A. Voth, P. Salvador, J.J. Dannenberg, V.G. Zakrzewski, S. Dapprich, A.D. Daniels, M.C. Strain, O. Farkas, D.K. Malick, A.D. Rabuck, K. Raghavachari, J.B. Foresman, J.V. Ortiz, Q. Cui, A.G. Baboul, S. Clifford, J. Cioslowski, B.B. Stefanov, G. Liu, A. Liashenko, P. Piskorz, I. Komaromi, R.L. Martin, D.J. Fox, T. Keith, M.A. Al-Laham, C.Y. Peng, A. Nanayakkara, M. Challacombe, P.M.W. Gill, B. Johnson, W. Chen, M.W. Wong, C. Gonzalez and J.A. Pople, *Gaussian03*, Gaussian, Inc., Pittsburgh, PA, 2003.

22. S. Hadisaputra, S. Hamdiani, M.A. Kurniawan and N. Nuryono, *Indones. J. Chem.*, 2017, **17**, no. 3, 431–438. doi: 10.22146/ijc.26667
23. R. Obayes, A. Al-Amiery, G. Alwan, A. Alobaidy, A. Al-Amiery, A. Kadhum and A. Mohamad., *Chem. Cent. J.*, 2014, **8**, no. 21, 1–8. doi: 10.1186/1752-153X-8-21
24. R. Obayes, A. Al-Amiery, G. Alwan, A. Alobaidy, A. Al-Amiery, A. Kadhum and A. Mohamad., *J. Mol. Struct*., 2017, **1138**, 27–34. doi: 10.1016/j.molstruc.2017.02.100
25. E. McCafferty and N. Hackerman, *J. Electrochem. Soc*., 1972, **119**, 146. doi: 10.1149/1.2404150
26. S.K. Shukla and E.E. Ebenso, *Int. J. Electrochem. Sci.*, 2011, **6**, 3277.
27. P. Luger, M. Weber, N.X. Dung, N.T.B. Tuyet., *Acta Cryst*. *C*, 1996, **45**, 1255–1257. doi: 10.1107/S0108270195016027
28. P. Senet, *Chem. Phys. Lett*., 1997, **275**, no. 5–6, 527–532. doi: 10.1016/S0009-2614(97)00799-9
29. I. Lukovits, E. Kalman and F. Zucchi, *Corrosion*, 2001, **57**, 3. doi: 10.5006/1.3290328

♦ ♦ ♦